Dinitrophenol-induced mitochondrial uncoupling in vivo triggers respiratory adaptation in HepG2 cells

Valérie Desquiret, Dominique Loiseau, Caroline Jacques, Olivier Douay, Yves Malthièry, Patrick Ritz, Damien Roussel*

Department of Biochemistry and Molecular Biology, INSERM UMR-694, 4 rue Larrey, F-49033 Angers cedex, France

Abstract

Here, we show that 3 days of mitochondrial uncoupling, induced by low concentrations of dinitrophenol (10 and 50 μM) in cultured human HepG2 cells, triggers cellular metabolic adaptation towards oxidative metabolism. Chronic respiratory uncoupling of HepG2 cells induced an increase in cellular oxygen consumption, oxidative capacity and cytochrome c oxidase activity. This was associated with an upregulation of COXIV and ANT3 gene expression, two nuclear genes that encode mitochondrial proteins involved in oxidative phosphorylation. Glucose consumption, lactate and pyruvate production and growth rate were unaffected, indicating that metabolic adaptation of HepG2 cells undergoing chronic respiratory uncoupling allows continuous and efficient mitochondrial ATP production without the need to increase glycolytic activity. In contrast, 3 days of dinitrophenol treatment did not change the oxidative capacity of human 143B.TK⁻ cells, but it increased glucose consumption, lactate and pyruvate production. Despite a large increase in glycolytic metabolism, the growth rate of 143B.TK⁻ cells was significantly reduced by dinitrophenol-induced mitochondrial uncoupling. We propose that chronic respiratory uncoupling may constitute an internal bioenergetic signal, which would initiate a coordinated increase in nuclear respiratory gene expression, which ultimately drives mitochondrial metabolic adaptation within cells.

1. Introduction

Mitochondrial oxidative phosphorylation produces most of the energy in aerobic living system by coupling respiration with the production of ATP. Respiration refers to the transfer of electrons from substrates to oxygen, a process that creates an electrochemical proton gradient across the inner mitochondrial membrane. The energy stored in this proton motive force is then used either by ATP synthase to synthesize ATP or by other proteins to drive ion and substrate transport. In addition, the electrochemical proton gradient can also be dissipated by proton leak reactions through either basal or inducible proton conductance pathways [1]. Inner mitochondrial membrane proton leakage is an ubiquitous phenomenon that diverts energy from ATP synthesis to thermogenesis, thereby modulating the yield of ATP synthesis in the mitochondria. It has been estimated that proton conductance accounts for a high proportion of cellular metabolic rate [1–3], causing up to 20% of standard metabolic rate in rats [2]. Accordingly, increased energy expenditure through increased mitochondrial proton leak has been proved to represent a treatment for obesity [4]. Mitochondrial proton conductance may also represent a mechanism for the regulation of mitochondrial reactive oxygen species production [5–8], mediators of oxidative cell damage. In association with this function, it has been suggested that mitochondrial proton leak

might play a protective role in atherosclerosis [9,10] and in the pathophysiology of diabetic complications [11]. Several other studies also support the role for mitochondrial uncoupling in the regulation of numerous other cellular metabolic functions such as calcium signaling [12,13], lipid/glucose metabolism [14–17] and beta cell glucose sensing [18]. These findings therefore suggest that mitochondrial proton leak might play a role in cellular metabolic homeostasis, which includes, but is not restricted to, the regulation of oxidative phosphorylation efficiency and heat production.

Recently, some independent studies have provided data, although scarce, suggesting that mitochondrial uncoupling constitutes an internal metabolic signal triggering mitochondrial biogenesis that could culminate in an adaptation of metabolic cell characteristics [19–21]. The aim of this work was to further characterize the role of chronic mitochondrial uncoupling in regulating cellular oxidative capacity and the possible cross-talk with the nuclear transcription factor and respiratory gene expression. We investigated the effect of 3 days of mitochondrial uncoupling induced by 2,4-dinitrophenol (DNP) on substrate metabolism, respiratory capacity, mitochondrial membrane potential and on the expression of nuclear respiratory factor-1 (NRF1) and the nuclear genes that encode mitochondrial proteins (COXIV, ANT2 and ANT3) in human HepG2 and 143B.TK⁻ cell lines. These two human cell lines were chosen as they differ in their energetic background, with HepG2 cells being more oxidative and thereby being less dependent on glycolytic ATP as a source of energy compared to 143B.TK⁻ cells. We found that uncoupling induced increased oxidative capacity in HepG2 cells, but not in 143B.TK⁻ cells. This was associated with an upregulation of HepG2 nuclear gene encoding COXIV and ANT3 proteins. The intracellular signaling pathways potentially involved in the reported causal link between mitochondrial uncoupling and adaptive changes in cellular respiratory function are discussed.

2. Materials and methods

2.1. Cell lines and growth conditions

The HepG2 human hepatoma cell line was grown in RPMI 1640 medium, supplemented with 10% fetal bovine serum (FBS), 2 mM L-glutamine, penicillin G (100 U/ml), streptomycin (2 mM) and amphoptericin B (0.25 µg/ml). The osteosarcoma-derived cell line (143.TK⁻) was grown in DMEM F12 with 10% FBS, 2 mM L-glutamine and the same antibiotics as used for HepG2 cells. Cells were seeded at a density of 15,000 cells per ml in a 20 ml flask were grown at 37 °C in a humidified atmosphere (5% CO₂–95% air) for 7 days in medium only (control) or in medium containing either 10 µM or 50 µM DNP. As DNP was made in ethanol solution, we used an experimental control condition, in which cells were grown in medium supplemented with ethanol (108 mM) only. Every 24 h (from J1 to J7), cells were collected by trypsinization and resuspended in PBS containing 5% FBS. An aliquot of each flask (control, ethanol, DNP 10 µM and DNP 50 µM) was colored using erythrosine to test cell viability. Then, three independent countings were done for each experimental culture condition. No differences in cell viability were found between DNP-treated and control cells, reinforcing the fact that the two concentrations of DNP used in the present work were not toxic towards HepG2 and 143B.TK⁻ cell lines [22].

Doubling time was determined for each culture condition (control, ethanol, DNP 10 µM and DNP 50 µM) using the exponential phase of the proliferation curve [log(cell number)=f(day of culture)] as follows:

$$\text{Doubling Time} = (T2 - T1)/[\ln(\text{cell number at } T2/\text{cell number at } T1)/\ln(2)]$$

where $(T2 - T1)$ is the duration of the exponential phase.

2.2. Measurement of oxygen consumption and FCCP titration of respiration in intact cells

After 3 days of culture, control and DNP-treated HepG2 and 143B.TK⁻ cells were collected by trypsinization and washed once in RPMI (HepG2) or DMEM (143B.TK⁻) containing 5% FBS and 2 mM L-glutamine. Two aliquots of each experimental condition were removed for cell counting. Then, the remaining cell suspensions were centrifuged (110 g for 5 min) and the pellet resuspended at a final concentration of 10×10^6 cells per ml (HepG2) or 5×10^6 cells per ml (143B.TK⁻) in 500 µl of the same medium supplemented with 2 mM L-glutamine (without FBS, DNP or ethanol) and previously air-equilibrated at 37 °C. The supernatants were collected and stored at −80 °C until assayed. The suspension was immediately transferred to the 1 ml chamber of a Clarke-type oxygen electrode (Rank Brothers Ltd.) maintained at 37 °C using a recirculating water bath and connected to a BD12E recorder model (Kipp and Zonen). Basal endogenous coupled respiration rate of cells was determined by measuring the linear rate of oxygen consumption, then oligomycin (12 µg/ml) was added and the non-phosphorylating respiration rate recorded. After recording the non-phosphorylating respiration rate, FCCP was added sequentially at different concentrations (ranging from 100 to 1000 nM for HepG2 cells and from 50 to 600 nM for 143B.TK⁻), and the uncoupled respiration rates measured. This titration was done because the uncoupling activity of FCCP in intact cells is biphasic, as shown in Fig. 1 for both hepatoma HepG2 and osteosarcoma 143B.TK⁻ cell lines. Therefore, we systematically achieved such a titration in order to determine the optimal FCCP concentration that gives maximal uncoupled respiration rate for each experimental condition.

Finally, myxothiazol (10 µM) was added to allow the measurement of non-mitochondrial oxygen consumption rate in cells. Myxothiazol inhibited rates were equally low in both untreated cell lines (6±2% of basal). In other words, mitochondria accounted for 94±2% of basal respiration in both untreated HepG2 and 143B.TK⁻ cell lines, and its contribution to total cell respiration rate was not significantly affected by DNP treatment (93±2% in 10 µM DNP-treated and 92±2% in 50 µM DNP-treated cells compared with 90±3% of control ethanol cells), excluding the possibility that non-mitochondrial oxygen consumption rates differed between experimental conditions. The oxygen solubility of the media was assumed to be 406 nmol O/ml. After recording the respiration rates, 400 µl of cell suspensions were collected from the chamber for total protein determination using the bicinchoninic acid procedure, with bovine serum albumin used as standard (BC Assay kit®, Montluçon, France).

Mitochondrial respiratory control ratio of cells was calculated as the ratio of oxygen consumed by mitochondria in the presence of FCCP to that in the presence of oligomycin, taking into account the myxothiazol rate $[(V_{\text{FCCP}} - V_{\text{myxo}})/(V_{\text{oligo}} - V_{\text{myxo}})]$. To determine the respiratory activity of mitochondria in intact cells, we expressed the basal endogenous respiration rate of mitochondria as a fraction of their maximal respiration $[(V_{\text{basal}} - V_{\text{myxo}})/(V_{\text{FCCP}} - V_{\text{myxo}})]$.

2.3. Measurement of mitochondrial membrane potential in intact cells

Cells were grown as already described for the oxygen consumption experiments. Three days after seeding, cells were collected by trypsinization and washed in PBS with 10% FBS. The cells were then resuspended in PBS, FBS 5%, 50 mM KCl and incubated with 20 nM cationic fluorescent dye DiOC6(3) in a 96-well plate (100,000 cells per well) for 30 min. In some wells, oligomycin (5 µg/ml) or mClCCP (10 µM) was added before incubation, either to inhibit ATP synthesis or to dissipate the proton gradient. After washing, the cells were set in tubes containing propidium iodide (8 µg/ml) to check membrane integrity. The fluorescent intensity was read using a flow cytometer (Becton-Dickinson). Laser excitation of DiOC6(3) was at 484 nm and emission was read at 511 nm.
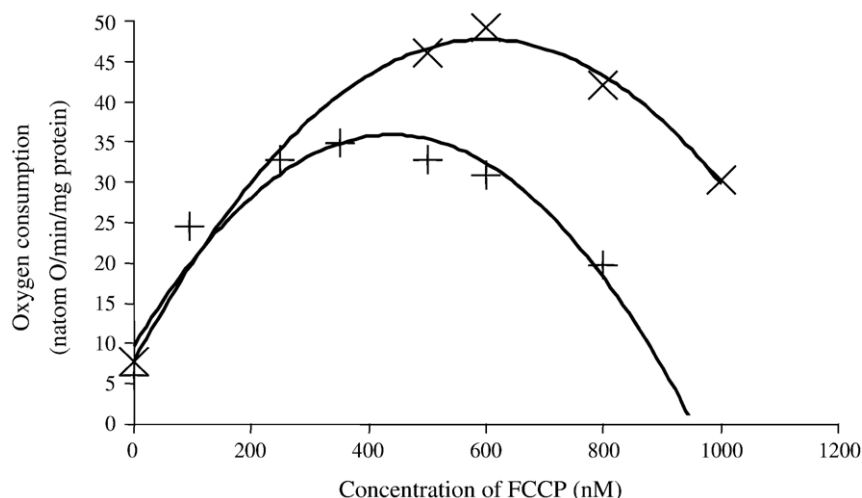
Fig. 1. Representative FCCP titration curves of non-phosphorylating oxygen consumption rate in HepG2 (×) and 143 B.TK⁻ cells (+). After endogenous respiration rate measurement and the addition of oligomycin (12 μg/ml), small amounts of FCCP were sequentially added in the polarographic chamber and a titration curve was drawn. See Materials and methods for further details.

Propidium iodide fluorescence was detected at 610 nm. Fluorescence analysis was performed using Cell Quest software.

2.4. Mitochondrial enzyme activities

Cytochrome c oxidase and citrate synthase activities were measured using standard spectrophotometric techniques [23]. The measurement of cytochrome c oxidase activity was performed in cells following three freezing/thawing cycles, by measuring decrease in absorbance resulting from the oxidation of reduced cytochrome c at 550 nm. Citrate synthase activity was measured in the same cells following the change in optical density of 5,5′-dithiobis(2-nitrobenzoic acid) at 412 nm. The activity of complex I (NADH:Ubiquinone oxidoreductase) was determined by monitoring the oxidation of NADH at 340 nm as described by Kuznetsov and Gnaiger [24]. Briefly, a pellet of 5×10^6 cells was resuspended in 250 μl PBS, froze in liquid nitrogen for 3 min. Then, frozen suspension was thawed and centrifuged at $16,000 \times g$ for 30 s. The pellet was resuspended in PBS at a final concentration of 1×10^6 cells per ml and sonicated on ice. An aliquot of the resultant suspension was added to a K-phosphate buffer containing 0.3 mM NADH, 0.1 mM Ubiquinone-1, 1 mM KCN and 2 mM NaN₃, pH 7.4 and the change in optical density of NADH was followed at 340 nm. After 120 s, rotenone (1 μM) was added to measure rotenone-insensitive activity of the preparation. Complex I activity was calculated as the total complex I activity minus the rotenone-insensitive activity.

2.5. RNA analysis and quantitative real-time RT PCR

Total RNA was extracted from frozen pellets of cells cultured for polarographic measurements (as described above) using the RNeasy Kit (Quiagen). Reverse transcription of 1 μg total RNA was performed in a total 20 μl volume. First, RNA was denatured at 70 °C for 2 min with oligo dT (20 pmol). Then, 5× reaction buffer (50 mM Tris–HCl, pH 8.3, 75 mM KCl and 3 mM MgCl₂), dNTPs mix (0.5 mM each), recombinant RNase inhibitor (1 U/μl) and MMLV reverse transcriptase (200 units/mg RNA) was added.

Samples were finally incubated at 37 °C for 1 h and 5 min at 94 °C. 30 μl of DEPC (treated with diethyl pyrocarbonate and autoclaved) water was added to the reaction mixture to obtain a final 50 μl reaction volume (RT for PCR kit, Clontech). cDNA previously synthesized were purified using the High Pure PCR Product Purification Kit (Boerhinger, Mannheim, Germany). Amplification products were then separated by gel (2.5% agarose) electrophoresis, stained with ethidium bromide, visualized and quantified using an integrating camera and analysis software (Molecular Analyst). Simultaneously, spectrophotometrical quantification was done by measuring optical density of samples at 260 nm (double strand DNA absorbancy wavelength) and 280 nm.

The levels of transcripts for adenine nucleotide translocator 2 (ANT2), ANT3, cytochrome c oxidase subunit IV (COXIV) and NRF1 were evaluated by quantitative real time RT PCR, using LightCycler™ (Roche Molecular Biochemicals, Mannheim, Germany) and LightCycler-RNA Amplification Kit SYBR Green I (Roche). Standard PCR products were generated by amplifying cDNA templates. Amplified fragments were then electrophoresed on agarose gels to confirm their expected size. Transcript levels were expressed in relation to that of acidic ribosomal phosphoprotein (ARP). PCR was performed using the following primers : ARP : 5′-CGA CCT GGA AGT CCA ACT AC-3′ (forward) and 5′-ATC TGC TGC ATC TGC TTG-3′ (reverse), ANT2 : 5′-GCT TGT GTA TGA TGA AA-3′ (forward) and 5′-AGA AAA CTG GTC AGA TGA AA-3′ (reverse), ANT3 : 5′-TCG AGA AAT TCC AGT TGT CTT T-3′ (forward) and 5′- AGA ACA CGA CTT GGC TCC TAC A-3′ (reverse), COXIV : 5′-TTG GCA AGC GAG CAA CC-3′ (forward) and 5′-TTC TCC TTC TCC TTC AAT GC-3′ (reverse), NRF1 : 5′-ATC TAT CCG GAA GAG GCA AC-3′ (forward) and 5′-GTG TTC TGC CAG AGC AGA CT-3′ (reverse).

2.6. Western blot analysis

Cells were grown, collected and counted as described above for the oxygen consumption experiments. Pellets of 5×10^6 cells were stored at −80 °C until used for western blot analysis. Frozen cells were lysated by an hypoosmotic shock (resuspension of the pellet in 96 μl of DEPC water and 4 μl of antiproteases). Protein concentration was determined by the Bio-Rad DC protein Assay kit (BioRad, Hercules, CA, USA). Whole-cell lysates were boiled for 10 min at 100 °C. Twenty micrograms of total protein were separated on a 12.5% SDS-polyacrylamide gel and electroblotted to a PVDF membrane (Amersham Biosciences, UK). Membranes were saturated with 5% non fat milk dissolved in TBS-Tween 0.1% (pH 7.4, NaCl 137 mM, KCl 2.7 mM, Tris 23 mM, Tween 20 0.1%) for 1 h at room temperature and incubated overnight at room temperature with monoclonal mouse anti-COXIV (1:5000 Interchim, Montluçon, France) and anti-VDAC (1:2500 Calbiochem, San Diego, USA). Membranes were then washed three times in TBS-Tween 0.1% and incubated with horseradish peroxidase-conjugated rabbit anti-mouse secondary antibody (1:10,000) for 1 h at room temperature. The immunoreactive proteins were visualized with enhanced chemiluminescence (ECL Western Blotting Detection Reagents, Amersham Biosciences, UK). Band intensities were quantified with Quantity One software (Bio-Rad).

2.7. Analysis of glucose, lactate and pyruvate

Glucose and lactate concentrations in the culture media were determined by spectrophotometry, using appropriate enzymatic kits (Boerhinger, Mannheim,

Germany) on a Hitachi-Roche apparatus (Roche Diagnostics GmbH, Mannheim, Germany). Pyruvate concentration was determined by measuring NADH concentration decrease in presence of the lactate dehydrogenase enzyme using spectrophotometry at a fixed wavelength of 340 nm. Glucose consumption and lactate and pyruvate production were normalized to total cellular protein content, as determined by the bicinchoninic acid assay kit (Uptima, Interchim, Montluçon, France) with bovine serum albumin as standard.

2.8. Statistical analysis

Statistics were performed by a one-way analysis of variance (ANOVA). A Scheffe's F test was subsequently used to test for differences between means. Statistical significance was recognized at $P < 0.05$. Values are presented as means ± S.E.M.

3. Results

3.1. Determination of cell growth

Fig. 2A shows that the total number of cells harvested after 7 days of culture did not differ between each experimental growth condition, suggesting that the proliferation rate of the HepG2 cell line remained unaffected by DNP treatment. This is confirmed by the fact that the doubling time of DNP-treated cells was similar to that of control cells (Fig. 2A, inset). Nevertheless, cells incubated in the presence of 50 μM DNP split up more slowly than control cells until 3 days after seeding, however, they then recovered the same proliferation rate as the control. Contrary to the HepG2 cell line, osteosarcoma-derived human cell line (143B.TK⁻) proliferation was inhibited by DNP treatment (Fig. 2B). The doubling time (Fig. 2B, inset) further indicated that the more DNP-induced mitochondrial uncoupling, the less 143B.TK⁻ grew. Thus, unlike HepG2 cells, 143B.TK⁻ cells were not able to recover normal growth when incubated in the presence of DNP. However, it is important to note that this inhibitory effect of DNP on 143B.TK⁻ cell proliferation was reversible, and when uncoupled cells were seeded again, without DNP, they grew at a rate similar to control cells (data not shown).

3.2. Glucose, lactate and pyruvate metabolism

Fig. 3 shows the effects of DNP treatment on glucose (panels A and B), lactate (panels C and D) and pyruvate (panels E and F) metabolism in both HepG2 (panels A, C and E) and 143B.TK⁻ cells (panels B, D and F). In HepG2 cell line, glucose consumption (Fig. 3A), lactate (Fig. 3C) and pyruvate production (Fig. 3E) were not significantly different between control and uncoupled cells. In 143B TK⁻ cells, contrary to the HepG2 cell line, glucose consumption ($R = 0.79$, $P < 0.0001$) and lactate production ($R = 0.91$, $P < 0.0001$) increased linearly with the intensity of DNP-induced mitochondrial uncoupling, reaching + 150% more in 50 μM DNP-treated 143B TK⁻ cells than in ethanol control cells, for both glucose consumption ($P < 0.05$, Fig. 3B) and lactate production ($P < 0.05$, Fig. 3D). Lactate production was also significantly and linearly related to glucose consumption ($R = 0.96$, $P < 0.0001$). The slope of the regression line was 1.73, which means that 87% of the glucose consumed was converted to lactate by glycolysis. This is calculated from the ideal maximal value of 2 for the ratio of lactate production/
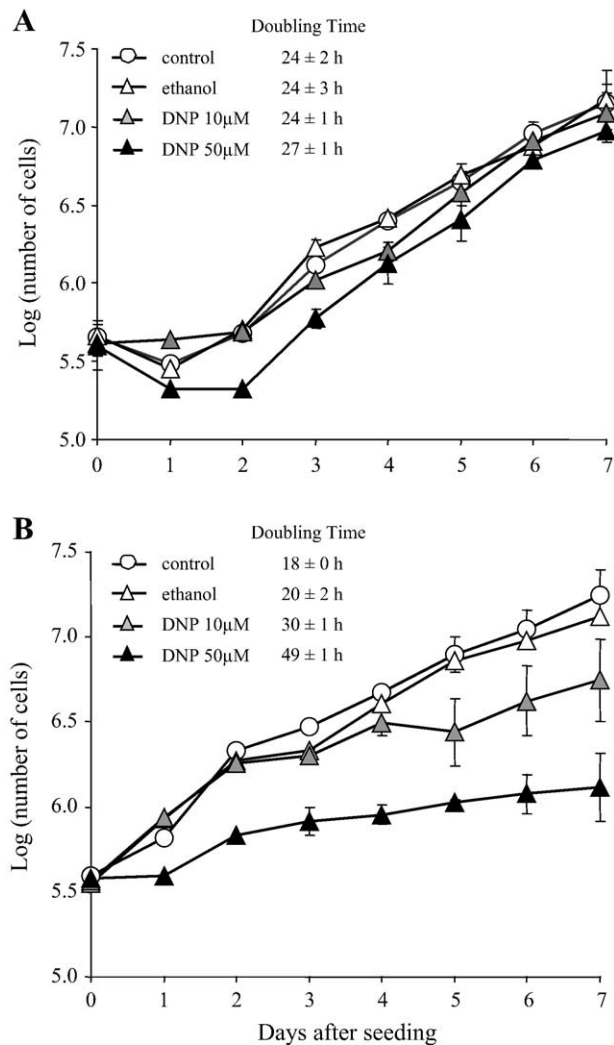

Fig. 2. Determination of cell growth. Cells were cultured for 7 days in control conditions (open circles), or in the presence of ethanol (open triangles), or treated with 10 μM DNP (gray triangles) or 50 μM DNP (black triangles). Every day, one flask was counted three times for each culture condition. After 7 days, a proliferation curve was drawn for HepG2 cells (A) and 143B TK⁻ cells (B) and the doubling time determined for each culture condition with the exponential phase of the curve. Values are expressed as means ± S.E.M. for $n = 2$ independent cell preparations.

glucose consumption, as in glycolysis 1 mol of glucose is converted into 2 mol of lactate. Finally, pyruvate was consumed by 143B.TK⁻ cells, except for cells incubated with DNP 50 μM, in which case pyruvate was produced in large amounts (Fig. 3F).

3.3. Mitochondrial membrane potential

The results shown in Fig. 4 are expressed as the percentage of cell fluorescence in relation to the fluorescence of ethanol control cells. In the two cells lines, mitochondrial membrane potential significantly decreased after cells were grown with DNP 10 μM for 3 days (−37% in HepG2 cell line and −23% in 143B TK⁻ cell line). When cells were grown in the presence of DNP 50 μM, a slight but not statistically significant 24% depolarization was noted in HepG2 cells ($P = 0.08$), whereas a significant 11% increase in fluorescence signal was found in
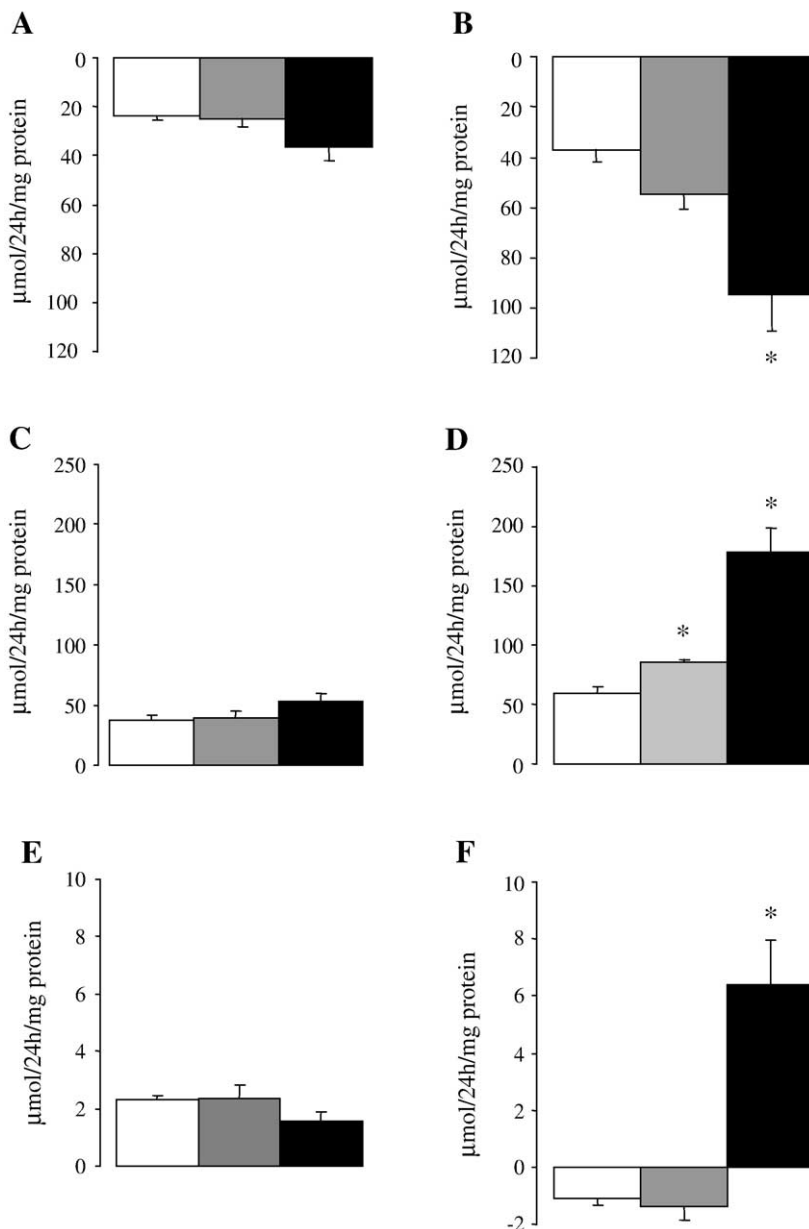
Fig. 3. Measurement of glucose, lactate and pyruvate concentrations. Three days after seeding, supernatant of cells in culture was removed and glucose (panels A and B), lactate (panels C and D) and pyruvate concentrations in media (panels E and F) were measured in both HepG2 (panels A, C and E) and 143B.TK− (panels B, D and F) for ethanol control cells (white bars), and for cells cultured in the presence of 10 μM DNP (gray bars) or 50 μM DNP (black bars). Values are expressed as means ± S.E.M., $n=5$ per group. $*P<0.05$ compared with control ethanol.

143B.TK− cells ($P<0.05$), suggesting a hyperpolarization of the membrane potential within cells.

3.4. Respiratory parameters of intact cells

The rates of basal endogenous respiration and FCCP-induced maximal respiration were approximately 50% and 75% higher in untreated HepG2 cells than in untreated 143B.TK− cells (18.0 ± 1.6 and 35.6 ± 3.5 natom O/min mg protein in HepG2 cells versus 12.1 ± 0.8 and 20.3 ± 1.5 natom O/min mg protein in 143B.TK− cells, respectively). We also noted a higher oligomycin-insensitive respiration rate in HepG2 (7.4 ± 0.8 natom O/min mg protein, $P<0.05$) than in 143B.TK− cells

(5.3 ± 0.5 natom O/min mg protein). However, respiratory control ratio of HepG2 cells was not significantly different from that of 143B.TK−, and in the basal state, mitochondria of both cell lines operated at an average of 56 ± 4% of maximal respiration.

Table 1 shows the effects of DNP treatment on the rates of basal endogenous respiration, oligomycin-insensitive respiration and FCCP-induced maximal respiration in both HepG2 and 143B TK− cell lines. The rate of basal endogenous respiration was significantly increased by approximately 30% in HepG2 cells treated with 50 μM DNP, an effect that was linearly correlated with DNP concentrations ($R=0.49$, $P<0.05$). Similarly, FCCP-induced maximal respiration rates significantly
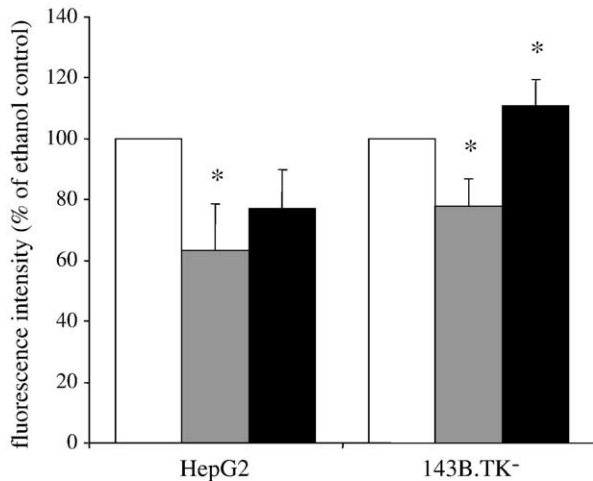
Fig. 4. Determination of mitochondrial membrane potential. Fluorescence of ethanol control (empty bars), DNP 10 µM (gray bars) and DNP 50 µM (black bars) cells pre-stained with DiOC6 (3) (20 nM) was determined by flow cytometry. Residual fluorescence emitted in the presence of 10 µM mClCCP was subtracted from the fluorescence of cells incubated with DiOC6(3) (20 nM) and oligomycin (5 µg/ml). Data is expressed as the percentage of fluorescence intensity of ethanol control values and expressed as means±S.E.M. for $n=3$ independent cell preparations measured in duplicate. *$P<0.05$ compared with ethanol control.

increased in HepG2 cells following 3 days of DNP treatment regardless of the concentration used, suggesting an overall stimulation of HepG2 respiratory capacity in response to DNP-induced mitochondrial uncoupling. Finally, DNP treatment did not significantly increase either the oligomycin-insensitive respiration rate of HepG2 cells nor any of the oxygen consumption rates (basal, oligomycin or FCCP) in 143B.TK⁻ cells. In fact, FCCP-uncoupled respiration rate of 143B.TK⁻ cells was rather decreased following 3 days of culture with DNP 50 µM, at least when compared with cell grown in the presence of 10 µM of DNP (−38%, $P<0.05$). Consequently, the respiratory control ratio of 143B.TK⁻ cells was lower following

3 days of treatment with DNP 50 µM compared with either ethanol control (−42%, $P<0.05$) or 10 µM DNP treated cells (−37%, $P=0.07$) (Table 1). In the basal state, we calculated that mitochondria of 143B.TK⁻ cells treated with 50 µM of DNP operated at $60\pm6\%$ of maximal respiration, a mitochondrial respiratory activity slightly higher than that observed in ethanol control ($43\pm5\%$, $P=0.07$) or 10 µM DNP-treated cells ($42\pm6\%$, $P=0.05$). In contrast, DNP treatment did not significantly alter respiratory control ratios of HepG2 cells (Table 1) nor the proportion of maximal respiratory activity used by mitochondria in intact cells ($55\pm3\%$ in ethanol control, $43\pm5\%$ in 10 µM DNP-treated, $45\pm4\%$ in 50 µM DNP-treated cells).

It must be emphasized here that all the respiratory parameters above were obtained in the absence of DNP, as cells were harvested and washed with incubation medium without DNP before experimental data were recorded. Hence, these results do reflect a true metabolic adaptation of cells to DNP-induced chronic mitochondrial uncoupling which is distinct from an acute effect of DNP on cell respiration.

3.5. Mitochondrial enzyme activities

Table 2 reports the enzymatic activities of citrate synthase and cytochrome c oxidase of HepG2 and 143B.TK⁻ cells for each experimental condition. Both mitochondrial enzyme activities were not affected by experimental conditions regardless of the cell line used, except for the enzymatic activity of COX, which was significantly increased in HepG2 cells cultured with DNP 50 µM ($P<0.05$). Table 2 also shows that the enzymatic activity of complex I in HepG2 cells was unaffected by the experimental conditions.

3.6. Expression of ANT3, COXIV, ANT2 and NRF1 genes

In HepG2 cells, 3 days of DNP treatment at 50 µM resulted in a marked induction of ANT3 and COXIV expression, whereas no significant change in both ANT2 and NRF1 mRNA levels was detected. Interestingly, a significant increase in COXIV mRNA levels was also detected in HepG2 cells after 3 days of incubation with only 10 µM DNP. In 143B.TK⁻ cells, none of the expression of the four genes considered was significantly affected following 3 days of DNP treatment, regardless of the concentration used (Table 3).

Table 1
Oxygen consumption rates of control ethanol and dinitropenol(DNP)-treated cells

Cell lines	Respiratory parameters	Treatments		
		Ethanol	DNP 10 µM	DNP 50 µM
HepG2	Basal respiration	15.1±0.7	16.9±0.7	20.3±1.5 *
	+oligomycin	6.5±0.6	7.9±0.8	8.1±0.8
	+FCCP	26.6±2.4	41.4±3.2 *	44.5±2.8 *
	RCR	4.9±0.4	5.3±1.0	5.9±0.5
143B.TK⁻	Basal respiration	9.7±0.6	11.7±1.1	10.4±0.6
	+oligomycin	5.0±0.4	6.5±0.7	6.2±0.3
	+FCCP	21.7±1.7	30.0±3.6	17.4±1.7
	RCR	5.5±0.9	5.1±0.7	3.2±0.4

Oxygen consumption rates were measured by polarography in the basal condition, in the presence of oligomycin (+oligomycin), and after the addition of FCCP (+FCCP). Respiration rates are expressed in natom of oxygen/min mg of protein. Respiratory control ratios (RCR) were calculated as the ratio between FCCP and oligomycin respiration rates, taking into account the myxothiazol rate. For more details see Materials and methods. Values are expressed as means±S.E.M. for $n=5$ independent cell preparations measured in duplicate.
 * $P<0.05$ compared with ethanol control treatment.

Table 2
Enzymatic measurements of cytochrome c oxidase, citrate synthase and complex I activities

Cell lines	Enzymes	Treatments		
		Ethanol	DNP 10 µM	DNP 50 µM
HepG2	Cytochrome c oxidase	37.3±6.9	38.1±6.9	51.4±3.3 *
	Citrate synthase	305.4±14.4	294.2±17.8	319.2±32.2
	Complex I	11.0±3.2	5.3±0.6	6.2±2.5
143B.TK⁻	Cytochrome c oxidase	20.2±4.2	26.1±2.3	21.6±1.4
	Citrate synthase	200.7±36.1	238.0±20.7	160.6±23.3

Cytochrome c oxidase, citrate synthase and complex I activities were determined by enzymatic measurements. Results are expressed in nmol/min mg of protein.
 * $P<0.05$ compared with ethanol control treatment.

Table 3
Quantification of *COXIV*, ANT3, *ANT2* and *NRF1* transcript levels

Cell lines	Genes	Treatments		
		Ethanol	DNP 10 μM	DNP 50 μM
HepG2	COXIV	0.09 ± 0.02	0.19 ± 0.02 *	0.18 ± 0.04 *
	ANT3	0.27 ± 0.04	0.28 ± 0.03	0.57 ± 0.06 *
	ANT2	0.29 ± 0.01	0.29 ± 0.05	0.32 ± 0.01
	NRF1	0.0031 ± 0.0002	0.0050 ± 0.0003	0.0020 ± 0.0010
143B.TK⁻	COXIV	0.08 ± 0.02	0.10 ± 0.01	0.08 ± 0.0
	ANT3	0.06 ± 0.00	0.06 ± 0.01	0.06 ± 0.01
	ANT2	0.63 ± 0.02	0.63 ± 0.05	0.65 ± 0.02
	NRF1	0.0062 ± 0.0010	0.0053 ± 0.0021	0.0041 ± 0.0022

Total RNA was extracted from cells following 3 days of culture in the presence of ethanol, 10 μM DNP or 50 μM DNP. After reverse transcription, quantitative RT PCR was performed to determine the level of gene transcripts as described in Materials and methods. Transcript levels were standardized with mRNA level of *ARP* gene. Values are expressed as means $\pm$ S.E.M. for $n = 3$ independent cell preparations measured in duplicate.

   * $P < 0.05$ compared with ethanol control.

3.7. Expression of COXIV protein

In HepG2 cells, the level of COXIV protein was significantly increased in HepG2 cells cultured with DNP 50 μM but not with DNP 10 μM (Fig. 5). In contrast, DNP treatment (10 or 50 μM) did not succeed in elevating COX protein level in 143B.TK⁻ cells (data not shown).

4. Discussion

The current work provides evidence that chronic mitochondrial uncoupling may constitute an internal bioenergetic signal that ultimately drives metabolic adaptation of HepG2 cells towards oxidative metabolism.

Indeed, we found that 3 days of DNP-induced mitochondrial uncoupling in HepG2 induced an increase in the rates of basal endogenous and FCCP-induced maximal oxygen consumption (Table 1), and in cytochrome *c* oxidase activity (Table 2). Additionally, the unchanged activity of citrate synthase suggests that the increased respiratory activity of uncoupled HepG2 cells did not result from an increased mitochondrial content, as the change in the activity of this marker enzyme of the citric acid cycle is widely accepted as being reliable and a valid indicator of changes in mitochondrial volume density [25]. This increased oxidative activity was associated with an upregulation of COXIV and ANT3 gene expression (Table 3), two nuclear genes that encode mitochondrial proteins involved in oxidative phosphorylation processes. Interestingly, the COXIV transcript level has been previously reported to increase in 3T3-L1 adipocytes after 10 h of incubation with 150 μM DNP or in mature adipocytes from transgenic mice expressing UCP1 in their white adipose tissue [20]. Furthermore, the increased COXIV transcript levels reported herein was associated with an increased COXIV protein expression (Fig. 5) showing that the reported increase in cytochrome *c* oxidase activity involves increased enzyme content. Villani et al. [26] have shown that there is a low reserve of COX activity in vivo in the respiratory chain of a variety of human cell types, including HepG2 cells.

This suggests that the in vivo control of respiration by COX is much tighter than has been assumed on the basis of experiments carried out on isolated mitochondria. In this regard, the present increase in the activity of COX has some significance for the overall capacity of mitochondrial oxidative phosphorylation in uncoupled HepG2 cells. Furthermore, the increase in the rate of FCCP-induced maximal oxygen consumption strongly suggests that other mitochondrial sites within the substrate oxidation pathways (e.g., respiratory chain complexes other than complex I (see Table 2), substrate dehydrogenases, substrate transport systems) are involved in DNP-induced metabolic adaptation of HepG2 cells. All these data clearly demonstrates that HepG2 cells develop their mitochondrial oxidative capacity in response to chronic mitochondrial uncoupling, a metabolic adaptation that allows HepG2 cells to produce energy efficiently to keep on growing (Fig. 2A), without the need to increase glycolytic activity (Fig. 3A and C).

As mentioned above, glucose consumption was not significantly changed in HepG2 cells following 3 days of DNP-induced mitochondrial uncoupling. However, mitochondrial membrane potential was depressed in uncoupled cells (Fig. 4), a situation where mitochondria, and by extension cells, should increase there substrate consumption. This relative discrepancy results from our choice to focus the present study on the effects of respiratory uncoupling upon glucose and glycolytic byproducts (lactate and pyruvate) rather than on oxidative substrate, namely glutamine that was also present in the culture media (see Materials and methods section). For this reason, the possibility cannot be excluded that glutamine, for instance, was indeed preferentially oxidized by uncoupled cells. This would be in line with previous observations showing that overexpression of uncoupling protein in cultured cells favours oxidative substrate (e.g. fatty acid) versus glucose oxidation [14,15]. Although we cannot substantiate this hypothesis, it should be noted that the present study clearly shows that chronic respiratory uncoupling
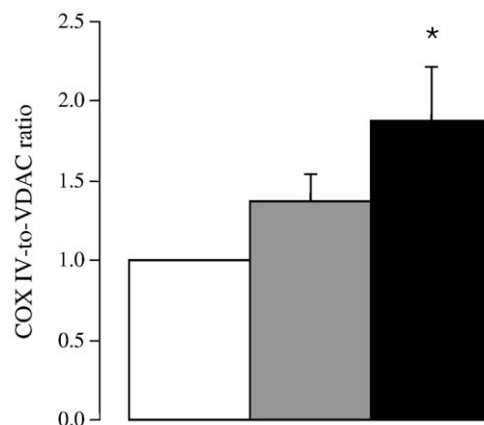

Fig. 5. Expression of COXIV protein in HepG2 cells. HepG2 cells were cultured in the presence of ethanol (white bar), 10 μM DNP (gray bar) or 50 μM DNP (black bar) for 3 days. Cellular extracts were subjected to Western blotting using VDAC and COXIV antibodies followed by densitometric quantitation of both proteins. Values are expressed relative to ethanol control ratio as means $\pm$ S.E.M. for $n = 4$ independent cell preparations measured in duplicate. *$P < 0.05$ compared with ethanol control.

of HepG2 cells by dinitrophenol leads to compensatory up-regulation of mitochondrial oxidative capacity.

Contrary to HepG2 cells, 3 days of DNP treatment did not change the oxidative capacity of 143B.TK⁻ cells, instead it increased their glycolytic metabolism. Thus, in 143B.TK⁻ cell lines, DNP treatment significantly increased glucose consumption (Fig. 3B) and lactate production (Fig. 3D) in a dose dependent manner. The strong positive correlation between glucose consumption and lactate production with a ratio lactate/glucose of almost 2:1 (measured by the slope of the regression line equation), indicating that most of the glucose uptake into uncoupled 143B.TK⁻ cells is reduced down the glycolytic pathway to produce energy. Nevertheless, despite this stimulation of glycolytic metabolism, the growth rate of 143B.TK⁻ cells was very sensitive to mitochondrial uncoupling, being significantly reduced by DNP treatment (Fig. 2B). Interestingly, treatment of 143B.TK⁻ cells with 50 µM DNP induced a slight but significant increase in the mitochondrial membrane potential which corresponded with a large stimulation of glycolysis and a drastic slow proliferation rate downwards. These results would be consistent with the fact that glycolytic ATP, the principal source of energy in 143B TK⁻ cells, may supply the energy for maintaining mitochondrial membrane potential and cell proliferation [27]. In the presence of 50 µM DNP, glycolysis may therefore not succeed in producing enough ATP to allow 143B.TK⁻ cells to grow efficiently while maintaining their mitochondrial membrane potential. Compared to HepG2 cell, our results show that the high

sensitivity to DNP-induced uncoupling in 143B.TK⁻ cells may be linked to their inability to develop mitochondrial energetic pathway to synthesize ATP.

The dual genomic organization of the mitochondrial oxidative phosphorylation complexes, which includes cytochrome *c* oxidase, implies that any adaptive change in mitochondrial characteristics must involve the coordinated expression of genes originating from both nuclear and mitochondrial genomes [28]. Therefore, the reported adaptive increase in mitochondrial oxidative activity of HepG2 in response to chronic respiratory uncoupling strongly suggests that a signaling pathway must originate from mitochondria, followed by the triggering of specialized transcription factors that initiate a coordinated increase in nuclear respiratory gene expressions (Fig. 6). Among the transcription factors, nuclear receptors and coactivators that regulate the expression of nuclear genes encoding mitochondrial proteins, NRF1 is the only one for which expression had been studied in response to respiratory uncoupling so far [19,20]. These studies reported that respiratory uncoupling increased the expression of NRF1 in HeLa cells 16 h after inducible expression of UCP1 [19] or in 3T3-L1 adipocytes incubated for 10 h with 150 µM DNP [20]. However, no significant change on NRF1 mRNA levels was observed in mature adipocytes isolated from 7-month-old transgenic mice expressing ectopic UCP1 in their white fat [20]. As far as our study is concerned, the levels of NRF1 mRNA were not significantly changed in HepG2 cells incubated for 3 days with either 10 µM or 50 µM DNP, despite an adaptive
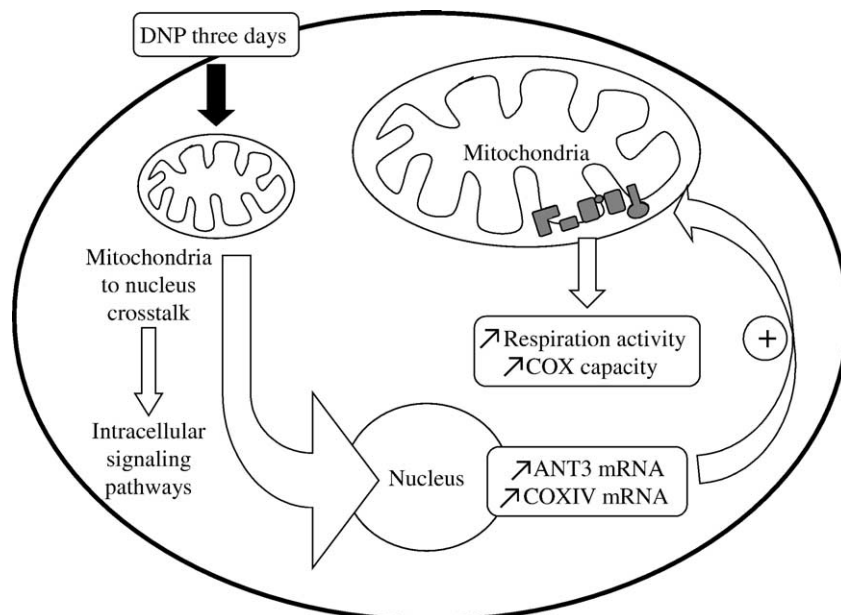

Fig. 6. Schematic diagram of the effect of chronic respiratory uncoupling on HepG2 cell metabolism. Three days of respiratory uncoupling induced by dinitrophenol (DNP) upregulates the expression of *COXIV* and *ANT3* genes and COXIV protein leading to increased mitochondrial oxidative activity in HepG2 cells. This metabolic adaptation of uncoupled HepG2 cells results from mitochondrial cross-talk with the expression of nuclear respiratory genes, implies that intracellular signaling pathway(s), followed by activation of specialized transcription factors initiates a coordinated expression of nuclear respiratory genes. At the onset of respiratory uncoupling, at least two rapid events have been described that could form part of the initial signaling process leading to activation of various transcription pathways: (1) lower cellular energy charge and the attendant increase in cytosolic AMP/ATP ratio [31,32] and (2) an increase in cytosolic calcium concentration [12,33]. The former event is known to activate AMP-activated protein kinase [31,34,35], and the second event can activate a number of kinases (e.g. calcium/calmodulin-dependent protein kinases, conventional protein kinase C) and phosphatases (e.g., calcineurine). These events would ultimately alter the expression of transcription factors and nuclear coactivators toward an adjustment in mitochondrial metabolism within cells [36–38].

increase in mitochondrial respiratory capacity (present study). The relative discrepancy between these studies may simply reveal the early molecular event that leads to mitochondrial differentiation or proliferation in response to changes in cellular bioenergetics. The hypothesis postulates that respiratory uncoupling triggers the immediate expression of NRF1 (within a few hours), followed by the up-regulation of NRF1-sensitive genes, such as ä-aminolevulinate synthase [19], cytochrome *c* and other nuclear genes required for respiratory chain expression and function [29]. This would contribute to the cellular energy metabolism adaptation and subsequent normalization of the initial signaling event that had induced NRF1 expression. Additionally, the increased COXIV transcript levels found in uncoupled cells (present study, see also [20]), a gene that is not sensitive to NRF1 [29,30], further suggests that other transcription factors, in particular NRF2 in this case, are likely to be involved in the stimulation of mitochondrial differentiation by respiratory uncoupling. We are currently working on this hypothesis in order to clarify whether the mitochondrial respiratory adaptation reported herein could be related to the early expression of NRF1 and other transcriptional activators (NRF2, mtTFA) and coactivators (PGC1, PRC). Finally, the present study provides evidence that modifications in mitochondrial bioenergetics influences the expression of nuclear genes which would in turn regulate mitochondrial characteristics and therefore cellular metabolism, at least in HepG2 (Fig. 6).

Acknowledgements

References

[1] J.A. Stuart, S. Cadenas, M.B. Jekabsons, D. Roussel, M.D. Brand, Mitochondrial proton leak and the uncoupling protein 1 homologues, Biochim. Biophys. Acta 1504 (2001) 144–158.

[2] D.F.S. Rolfe, J.M.B. Newman, J.A. Buckingham, M.G. Clark, M.D. Brand, Contribution of mitochondrial proton leak to respiration rate in working skeletal muscle and liver and to SMR, Am. J. Physiol. 276 (1999) C692–C699.

[3] S. Krauss, C.Y. Zhang, B.B. Lowell, A significant portion of mitochondrial proton leak in intact thymocytes depends on expression of UCP2, Proc. Natl. Acad. Sci. U. S. A. 99 (2002) 118–122.

[4] J.A. Harper, K. Dickinson, M.D. Brand, Mitochondrial uncoupling as a target for drug development for the treatment of obesity, Obes. Rev. 2 (2001) 255–265.

[5] K.S. Echtay, D. Roussel, J. St-Pierre, M.B. Jekabsons, S. Cadenas, J.A. Stuart, J.A. Harper, S.J. Roebuck, A. Morrison, S. Pickering, J.C. Clapham, M.D. Brand, Superoxide activates mitochondrial uncoupling proteins, Nature 415 (2002) 96–99.

[6] A. Nègre-Salvayre, C. Hirtz, G. Carrera, R. Cazenave, M. Troly, R. Salvayre, L. Pénicaud, L. Casteilla, A role for uncoupling protein-2 as a regulator of mitochondrial hydrogen peroxide generation, FASEB J. 11 (1997) 809–815.

[7] A.J. Vidal-Puig, D. Grujic, C.Y. Zhang, T. Hagen, O. Boss, Y. Ido, A. Szczepanik, J. Wade, V. Mootha, R. Cortright, D.M. Muoio, B.B. Lowell, Energy metabolism in uncoupling protein 3 gene knockout mice, J. Biol. Chem. 275 (2000) 16258–16266.

[8] D. Arsenijevic, H. Onuma, C. Pecqueur, S. Raimbault, B.S. Manning, B. Miroux, E. Couplan, M.C. Alves-Guerra, M. Goubern, R. Surwit, F. Bouillaud, D. Richard, S. Collins, D. Ricquier, Disruption of the uncoupling protein-2 gene in mice reveals a role in immunity and reactive oxygen species production, Nat. Genet. 26 (2000) 435–439.

[9] C. Bernal-Mizrachi, S. Weng, B. Li, L.A. Nolte, C. Feng, T. Coleman, J.O. Holloszy, C.F. Semenkovich, Respiratory uncoupling lowers blood pressure through a leptin-dependent mechanism in genetically obese mice, Arterioscler. Thromb. Vasc. Biol. 22 (2002) 961–968.

[10] J. Blanc, M.C. Alves-Guerra, B. Esposito, S. Rousset, P. Gourdy, D. Ricquier, A. Tedgui, B. Miroux, Z. Mallat, Protective role of uncoupling protein 2 in atherosclerosis, Circulation 107 (2003) 388–390.

[11] M. Brownlee, Biochemistry and molecular cell biology of diabetic complications, Nature 414 (2001) 813–820.

[12] D. Hudman, R.D. Rainbow, C.L. Lawrence, N.B. Standen, The origin of calcium overload in rat cardiac myocytes following metabolic inhibition with 2,4-dinitrophenol, J. Mol. Cell. Cardiol. 34 (2002) 859–871.

[13] Z.A. Khayat, T. Tsakiridis, A. Ueyama, R. Somwar, Y. Ebina, A. Klip, Rapid stimulation of glucose transport by mitochondrial uncoupling depends in part on cytosolic Ca^{2+} and cPKC, Am. J. Physiol. 275 (1998) C1487–C1497.

[14] C. Garcia-Martinez, B. Sibille, G. Solanes, C. Darimont, K. Macé, F. Villarroya, A.M. Gomez-Foix, Overexpression of UCP3 in cultured human muscle lowers mitochondrial membrane potential, raises ATP/ADP ratio, and favors fatty acid vs. glucose oxidation, FASEB J. 15 (2001) 2033–2035.

[15] Y. Hong, B.D. Fink, J.S. Dillon, W.I. Sivitz, Effects of adenoviral overexpression of uncoupling protein-2 and -3 on mitochondrial respiration in insulinoma cells, Endocrinology 142 (2001) 249–256.

[16] M. Rossmeisl, I. Syrovy, F. Baumruk, P. Flachs, P. Janovska, J. Kopecky, Decreased fatty acid synthesis due to mitochondrial uncoupling in adipose tissue, FASEB J. 14 (2000) 1793–1800.

[17] C. Huppertz, B.M. Fischer, Y.B. Kim, K. Kotani, A. Vidal-Puig, L.J. Slieker, K.W. Sloop, B.B. Lowell, B.B. Kahn, Uncoupling protein 3 (UCP3) stimulates glucose uptake in muscle cells through a phosphoinositide 3-kinase-dependent mechanism, J. Biol. Chem. 276 (2001) 12520–12529.

[18] C.Y. Zhang, G. Baffy, P. Perret, S. Krauss, O. Peroni, D. Grujic, T. Hagen, A.J. Vidal-Puig, O. Boss, Y.B. Kim, X.X. Zheng, M.B. Wheeler, G.I. Shulman, C.B. Chan, B.B. Lowell, Uncoupling protein-2 negatively regulates insulin secretion and is a major link between obesity, beta cell dysfunction, and type 2 diabetes, Cell 105 (2001) 745–755.

[19] B. Li, J.O. Holloszy, C.F. Semenkovich, Respiratory uncoupling induces ä-aminolevulinate synthase expression through a nuclear respiratory factor-1-dependent mechanism in HeLa cells, J. Biol. Chem. 274 (1999) 17534–17540.

[20] M. Rossmeisl, G. Barbatelli, P. Flachs, P. Brauner, M.C. Zingaretti, M. Marelli, P. Janovska, M. Horakova, I. Syrovy, S. Cinti, J. Kopecky, Expression of the uncoupling protein 1 from the aP2 gene promoter stimulates mitochondrial biogenesis in unilocular adipocytes in vivo, Eur. J. Biochem. 269 (2002) 19–28.

[21] E. Couplan, C. Gelly, M. Goubern, C. Fleury, B. Quesson, M. Silberberg, E. Thiaudière, P. Mateo, M. Lonchampt, N. Levens, C. de Montrion, S. Ortmann, S. Klaus, M. Gonzalez-Barroso, A.M. Cassard-Doulcier, D. Ricquier, A.X. Bigard, P. Diolez, F. Bouillaud, High level of uncoupling protein 1 expression in muscle of transgenic mice selectively affects muscles at rest and decreases their IIb fiber content, J. Biol. Chem. 277 (2002) 43079–43088.

[22] M.Y. Moridani, A. Siraki, P.J. O'Brien, Quantitative structure toxicity relationships for phenols in isolated rat hepatocytes, Chem.-Biol. Interact. 145 (2003) 213–223.

[23] S. Horie, M. Morrison, Cytochrome c oxidase components. I. Purification and properties, J. Biol. Chem. 238 (1963) 1855–1860.

[24] A.V. Kuznetsov, E. Gnaiger, Laboratory Protocol. Complex I (NADH: Ubiquinone oxidoreductase, EC 1.6.5.3) mitochondrial membrane enzyme, MiTNet 8.15 (2003) 1–8.

[25] J.O. Holloszy, E.F. Coyle, Adaptations of skeletal muscle to endurance

exercise and their metabolic consequences, J. Appl. Physiol. 56 (1984) 831–838.

[26] G. Villani, M. Greco, S. Papa, G. Attardi, Low reserve of cytochrome *c* oxidase capacity in vivo in the respiratory chain of a variety of human cell types, J. Biol. Chem. 273 (1998) 31829–31836.

[27] A. Chevrollier, D. Loiseau, F. Gautier, Y. Malthiery, G. Stepien, ANT2 expression under hypoxic conditions produces opposite cell-cycle behavior in 143B and HepG2 cancer cells, Mol. Carcinog. 42 (2005) 1–8.

[28] C.D. Moyes, D.A. Hood, Origins and consequences of mitochondrial variation in vertebrate muscle, Annu. Rev. Physiol. 65 (2003) 177–201.

[29] R.C. Scarpulla, Nuclear activators and coactivators in mammalian mitochondrial biogenesis, Biochim. Biophys. Acta 1576 (2002) 1–14.

[30] K. Baar, Z. Song, C.F. Semenkovich, T.E. Jones, D.H. Han, L.A. Nolte, E. O. Ojuka, M. Chen, J.O. Holloszy, Skeletal muscle overexpression of nuclear respiratory factor 1 increases glucose transport capacity, FASEB J. 17 (2003) 1666–1673.

[31] O. Matejkova, K.J. Mustard, J. Sponarova, P. Flachs, M. Rossmeisl, I. Miksik, M. Thomason-Hughes, D.G. Hardie, J. Kopecky, Possible involvement of AMP-activated protein kinase in obesity resistance induced by respiratory uncoupling in white fat, FEBS Lett. 569 (2004) 245–248.

[32] G. Cheng, C.C. Polito, J.K. Haines, S.F. Shafizadeh, R.N. Fiorini, X. Zhou, M.G. Schmidt, K.D. Chavin, Decrease of intracellular ATP content downregulated UCP2 expression in mouse hepatocytes, Biochem. Biophys. Res. Commun. 308 (2003) 573–580.

[33] C.J. Lynch, R.C. Deth, Release of a common source of intracellular Ca^{2+} by alpha-adrenergic agonists and dinitrophenol in rat liver slices, Pharmacology 28 (1984) 74–85.

[34] T. Hayashi, M.F. Hirshman, N. Fujii, S.A. Habinowski, L.A. Witters, L.J. Goodyear, Metabolic stress and altered glucose transport activation of AMP-activated protein kinase as a unifying coupling mechanism, Diabetes 49 (2000) 527–531.

[35] N. Patel, Z.A. Khayat, N.B. Ruderman, A. Klip, Dissociation of 5(AMP-activated protein kinase activation and glucose uptake stimulation by mitochondrial uncoupling and hyperosmolar stress : differential sensitivities to intracellular calcium and protein kinase C inhibition, Biochem. Biophys. Res. Commun. 285 (2001) 1066–1070.

[36] W.W. Winder, Energy-sensing and signaling by AMP-activated protein kinase in skeletal muscle, J. Appl. Physiol. 91 (2001) 1017–1028.

[37] E.O. Ojuka, T.E. Jones, D.H. Han, M. Chen, J.O. Holloszy, Raising Ca^{2+} in L6 myotubes mimics effects of exercise on mitochondrial biogenesis in muscle, FASEB J. 17 (2003) 675–681.

[38] D. Freyssenet, I. Irrcher, M.K. Connor, M. Di Cario, D.A. Hood, Calcium-regulated changes in mitochondrial phenotype in skeletal muscle ells, Am. J. Physiol. 286 (2004) C1053–C1061.